Publications of the Astronomical Society of the Pacific, 130:125001 (12pp), 2018 December https://doi.org/10.1088/1538-3873/aae2f7

Calibration Tests of a 25-GHz Mode-spacing Broadband Astro-comb on the Fiber-fed High Resolution Spectrograph (HRS) of the Chinese 2.16-m Telescope

Zhibo Hao[1,2,3], Huiqi Ye[1,2], Jian Han[1,2], Yuanjie Wu[1,2], Yang Zhai[1,2], and Dong Xiao[1,2]
[1] National Astronomical Observatories/Nanjing Institute of Astronomical Optics & Technology, Chinese Academy of Sciences, Nanjing 210042, People's Republic of China; dxiao@niaot.ac.cn
[2] CAS Key Laboratory of Astronomical Optics & Technology, Nanjing Institute of Astronomical Optics & Technology, Nanjing 210042, People's Republic of China
[3] University of Chinese Academy of Sciences, Beijing 100049, People's Republic of China
Received 2018 August 16; accepted 2018 September 17; published 2018 October 19

Abstract

A 25-GHz mode-spacing astro-comb with 470–720 nm wavelength coverage has been installed as the calibration source on the fiber-fed High Resolution Spectrograph (HRS) of the Chinese 2.16-m telescope at Xinglong Observatory. The calibration tests were carried out based on the single-channel system of HRS. The results have achieved a 2–8 times (for different orders) higher wavelength solution accuracy than the thorium argon (ThAr) lamp, and a short-term repeatability of 0.1 m s^{-1}, which is around the photon noise limit. It proved that the coupling system linking the astro-comb to HRS successfully suppressed the negative effects of laser speckles. The comb-line overlapping exists in the acquired spectrum of the astro-comb on HRS. We demonstrated that when determining the comb-line center, the comb-line overlapping leads to a systematic bias, which is caused by asymmetrical sampling, and meanwhile a larger uncertainty. The correction for the systematic bias is feasible by simulating the overlapping comb lines according to actual comb-line spacing and pixel phase and then calculating the difference of the fitted line center with the true line center. A higher accuracy of wavelength solution has been achieved after correction.

Key words: astro-comb – laser frequency comb – techniques: radial velocities – techniques: spectroscopic – methods: data analysis

Online material: color figures

1. Introduction

The demand of highly stable and precise measurement of the scientific target's radial velocity (RV) via the Doppler method is growing in some of the most important astrophysical research, such as detecting Earth-mass exoplanets around solar-mass stars in the habitable zone (5 cm s^{-1} precision stable over years), and directly measuring the universe's expansion history i.e., Sandage-Loeb experiment (1 cm s^{-1} precision stable over tens of years) (Steinmetz et al. 2008). Highly accurate wavelength calibration of high-resolution spectrum plays a key role in the frontier studies of the stellar or galactic metallicity (Skidmore et al. 2015). All of those demands call for extremely stable, precise, and accurate wavelength calibration sources for the spectrograph. Nevertheless, the traditional calibration sources face some crucial drawbacks. For example, an iodine absorption cell has a narrow wavelength coverage, and the absorption reduces the scientific target's signal; thorium argon (ThAr) hollow-cathode lamp has the characteristics of irregular line spacing, bleeding of strong lines, and long-term spectral drifting (Probst 2015). To meet those demands, innovative calibration sources have been developed. Among them, astro-combs are perfect candidates for their preferable performances (Steinmetz et al. 2008; Wilken et al. 2010, 2012; Phillips et al. 2012; Doerr et al. 2012; Ycas et al. 2012).

Astro-comb can offer a series of narrow, regularly spaced emission lines (comb teeth) in the frequency domain, with a rather wide wavelength coverage. When locked to a standard radio-frequency reference, the comb teeth are stabilized to a precision approaching 10^{-12} for any length of time (Charsley et al. 2017). The frequency of comb teeth can be accurately determined by the formula of $f_n = f_0 + nf_{\rm rep}$, where f_0 denotes the offset frequency, $f_{\rm rep}$ denotes the repetition rate (also known as the mode spacing), and n denotes the mode number. Several repetition rates in the range of 5.5–50 GHz have been realized to fit for different resolution of the spectrographs (McCracken et al. 2017a). With those characteristics, astro-comb is able to meet the requirement of extreme stability, precision, and accuracy of the calibration source for the next generation spectrograph to support the development of advanced astronomy.

The fiber-fed High Resolution Spectrograph (HRS) of the Chinese 2.16-m telescope at Xinglong Observatory is the main RV instrument in China. HRS has contributed to the finding of two exoplanets (Wang et al. 2014; Sato et al. 2016), several brown dwarfs, and substellar companions (Liu et al. 2008, 2009; Wang et al. 2012) in the planet-search collaborative program between Japan and China. To improve the calibration performance of HRS, and to explore the pilot research of RV detection techniques aimed at the level of cm s^{-1}, the study of the astro-comb on HRS has begun. The astro-comb, product of Menlo Systems GmbH, was installed on the HRS in 2016. It has a repetition frequency of 25 GHz and a broad wavelength range of 470–720 nm, covering most of the visible region.

Although the intrinsic stability, precision, and accuracy of the astro-comb are extremely high, the calibration performance will be worsened when the astro-comb practically applied to its host spectrograph, caused not only by the limited resolution, which smooths and pixelates the comb lines' spectral profiles, thus fundamentally reduces the calibration signal, but also by other factors: the aberration of the optical system, the intra-pixel sensitivity variation, the instability of the spectrograph environment, and so on. Murphy et al. (2007) introduced a method to estimate the loss of precision caused by limited resolution. However, the effect of some other factors can hardly be anticipated or exactly estimated. Thus, calibration tests are indispensable in evaluating the practical performance with the implementation of the astro-comb on a spectrograph. Phillips et al. (2012) showed a repeatability of 50 cm s^{-1} on TRES with the astro-comb of 50-GHz mode spacing from 400 to 420 nm. Probst et al. (2016) demonstrated a repeatability of 2.8 cm s^{-1} on HARPS with the astro-comb of 18-GHz mode spacing which covers the whole spectral range of HARPS from 460 to 690 nm. They are all in good agreement with photon noise limit. On the other hand, Probst et al. (2015) displayed a repeatability at the level of 10 cm s^{-1} on VTT echelle spectrograph with the astro-comb of 5.445-GHz mode spacing and 0.7 nm wide spectral range centered at 630.0 nm, which is larger than the photon noise limit by a factor of 1.34. The excess part was considered that it is most likely to be provoked by internal seeing within the spectrograph beam path. For absolute calibration, the tests performed by Molaro et al. (2013) on HARPS revealed the negative effect of CCD stitching pattern. After correction the error of wavelength solution was suppressed to about 3 m s^{-1} rms. Those calibration tests demonstrated the astro-comb's function as a diagnostic tool with the ability to study the factors which influence the calibration performance. Both the next generation spectrographs and the currently operating spectrographs can benefit from the use of astro-comb. This paper will present our calibration tests of the astro-comb on HRS.

A brief system description is presented in Section 2. Section 3 is dedicated to the data analysis of the calibration tests, including absolute calibration and repeatability test. A brief summary is given in Section 4.

2. System Description

The HRS is mounted in the spectrograph room of the 2.16-m telescope. A multi-mode optical fiber (MMF) transmits the light of the scientific target from the Cassegrain unit to the spectrograph. It can be switched between an MMF with 100 μm core-diameter, which is currently in position, and another MMF with 62.5 μm core-diameter. The wavelength coverage is 370–920 nm, and the average resolution is 50,000 for the 100 μm MMF. The main body of HRS is sealed in a protective chamber with the temperature stability of ± 0.05°C per night (Fan et al. 2016). The detector is a 16-bit back-illuminated E2V CCD (203–82), with a size of 4096 × 4096 pixels and a pixel-size of 12 μm. An iodine absorption cell and a ThAr lamp are both installed for wavelength calibration, and can be switched for different scientific goals. The precision of RV measurements can reach 6 m s^{-1} rms (Zhao et al. 2014).

The astro-comb on HRS has a Yb-fiber source comb of a mode spacing of 250 MHz, operating at a center wavelength of 1040 nm and using the Global Positioning System (GPS) as the radio-frequency reference. The mode spacing increases to 25 GHz by mode filtering through a series of three identical Fabry-Pérot cavities with a finesse of 2300 (Wu et al. 2016). The transmitted comb teeth are subsequently compressed with a pair of grating and then broadened in spectrum with a tapered photonic crystal fiber to cover the visible light region. Finally, the broadened spectrum is flattened to have uniform flux over the whole wavelength range. This astro-comb is very similar to the one installed on FOCES spectrograph of the 2 m Fraunhofer telescope at Wendelstein Observatory, which is also the product of Menlo System GmbH (Brucalassi et al. 2016; Wang et al. 2016).

Due to the highly temporal and spatial coherence, the laser speckles will be produced by modal interference when coupling the astro-comb light through MMF. The speckle pattern is very susceptible to the motion or deformation of MMF. The variation of speckle pattern will result in the shift of the centroid of Line Spread Function (LSF) of the spectrograph (Probst 2015). Thus, a coupling system linking the astro-comb with HRS has been set up to carry out the dynamic scrambling, using a vibrator attached to the MMF to eliminate the laser speckles by rapid vibration (Ye et al. 2016). In addition, octagonal-cored MMFs are used as static scrambler to homogenize the spatial mode occupation of fiber globally. The output light of the octagonal-cored MMFs is coupled into the MMF of HRS through an F-conversion unit for matching the focal ratio to be the same with that of the telescope. There are filter mounts and a shutter in the F-conversion unit. They can be used to adapt the intensity of the astro-comb light to different conditions.

3. Calibration Tests

In this section, we will describe our method and results of the calibration tests. Before that, we briefly introduce our data

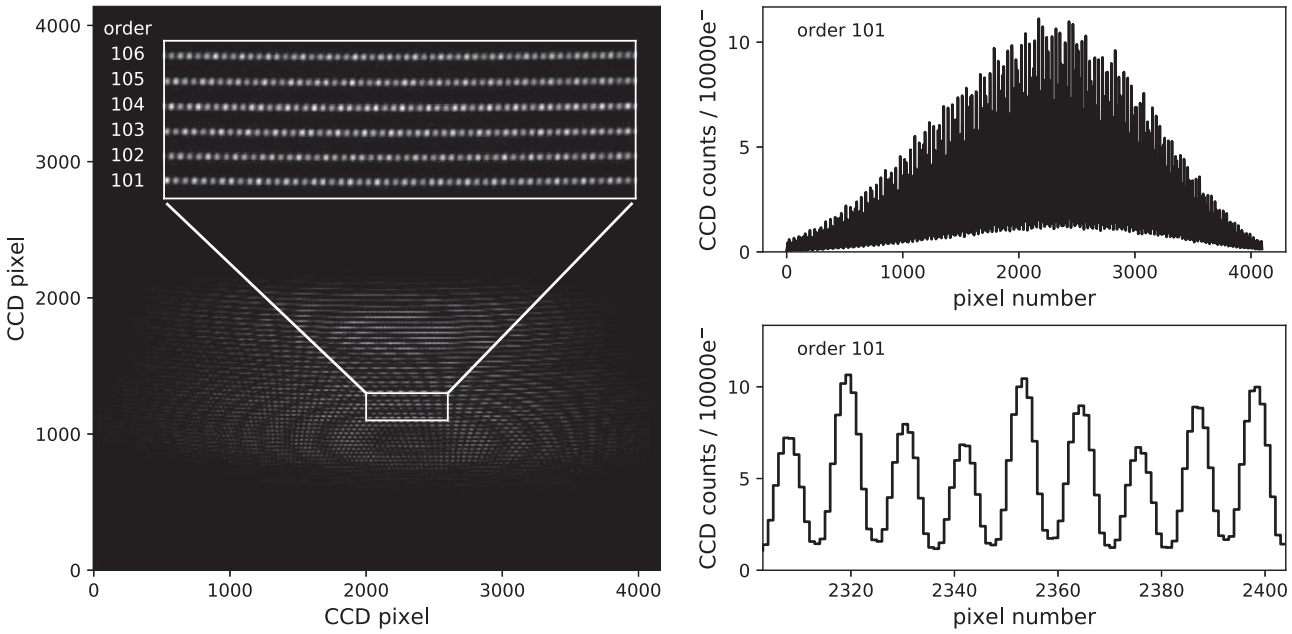

Figure 1. Left: raw 2D spectrum of the astro-comb on HRS, with the subfigure to magnify the spectral feature. The order numbers of the subfigure are mentioned. Upper right: the extracted 1D spectrum of order 101. Lower right: a portion of the extracted 1D spectrum of order 101. The comb-line overlapping can be noted.

reduction process. IRAF[4] is used to carry out the data reduction, and some Python programs have also been developed to provide auxiliary support. After bias subtraction, order tracing, and background correction, the 1D spectrum is extracted by summing 14 pixels of every column perpendicular to the dispersion direction. Based on the 1D spectrum, the positions of the comb lines are detected by the Python peak finding program. The astro-comb's spectrum covers from order 82 (long wavelength end) to order 124 (short wavelength end) of HRS. When the astro-comb light is adequately exposed (maximum signal-to-noise ratio (S/N) of 200 per CCD physical pixel), about 14,000 comb teeth can be detected in a single exposure (including the repetitive spectral range of the orders).

HRS is originally of single-channel design. Later, the simultaneous calibration channel was added by adding another fiber adjacent to the science fiber at the slit. Although some optimization has been carried out, a moderate extent of crosstalk between the two channels still exits. To resolve the problem of channel crosstalk, further adjustments still need to be made. Thus, the current calibration tests in this paper are all based on the single-channel system.

The left panel of Figure 1 shows the raw 2D spectrum of the astro-comb recorded with HRS. The upper-right panel and the lower-right panel show the whole and partial extracted 1D spectrum of order 101. It can be seen that the comb lines are not dispersed enough to separate the adjacent comb lines completely, i.e., the adjacent comb lines overlap with one another. This is because the resolution of HRS is relatively low under the 25-GHz mode spacing of the astro-comb. The comb-line overlapping is even more severe for higher diffraction orders, due to their decreased resolution. The comb-line overlapping will result in some loss of accuracy and precision. Detailed investigation of it will be given in the following subsections.

3.1. Absolute Calibration

3.1.1. Basic Method and Results

The astro-comb and the ThAr lamp are both emission-line-type calibration sources. Comparing with the atlas of the ThAr spectrum, the atlas of the astro-comb spectrum is less complicated thanks to its regularly spaced emission lines. In principle, it should be easier to finish the absolute calibration.

Here, a linear-polynomial-added Gaussian function is used to fit each comb line to determine the line center (Probst et al. 2016):

$$f(x) = a_1 + a_2 x + a \exp\left(-\frac{(x-\mu)^2}{2\sigma^2}\right), \quad (1)$$

where x denotes the pixel position, and other symbols denote the fitting parameters. The Gaussian function is used to fit the LSF of HRS. The linear polynomial is used to fit the slope structure of the spectral background. The noise of each data point follows the photon noise assumption, $\sqrt{(\sqrt{N})^2 + R^2}$,

[4] Image Reduction and Analysis Facility, which is distributed by the National Optical Astronomy Observatories (NOAO; Tody 1993).

where N denotes the number of counts at this pixel ($\sqrt{N}$ is the value of photon noise), and R denotes the CCD readout noise. In the case of HRS, $R^2 = 14 \times 2.75^2 = 105.875$. (The readout noise for each CCD physical pixel is 2.75). The fitted μ is defined as the line center. σ_μ (the uncertainty of μ), which can be obtained from the Jacobian matrix, is also saved for further analysis.

The mode number, frequency, and wavelength of each comb line can be identified by comparing the spectrum of astro-comb with the spectrum of ThAr lamp exposed before or after, just as the method in Phillips et al. (2012). Then, the wavelength solution $\lambda = \lambda_o(x)$ is calculated by performing a fifth-order polynomial fit of the relation between the line center and the wavelength for each order.

The upper panel of each order in Figure 2 shows the residuals from the fitted function. The solid dots are the comb lines used for fitting, while the hollow dots are outliers by σ-clipping criterion with $\sigma_{\rm clip} = 3$. It shows an average 0.00085 Å (43 m s^{-1})[5] rms error for these five orders, which is a significant improvement with respect to the former ThAr lamp calibration result of 0.003 Å (150 m s^{-1}). The residuals for ThAr lamp lines from the fitted function are plotted in the same panels of Figure 2, shown in red dots. These data are reduced from the exposure of ThAr lamp that was taken immediately after the exposure of the astro-comb using the atlas provided by IRAF, and refined by the atlas provided by Redman et al. (2014). The error bars are determined by the propagation of the measured wavenumber uncertainty from Table 6 in Redman et al. (2014) and the photon-noise-induced uncertainty in the emission-line fitting. It shows an average 0.00144 Å (72 m s^{-1}) rms error, improving by a factor of two compared with 0.003 Å (150 m s^{-1}). The two-fold improvement is in accord with the result of McCracken et al. (2017b), who refined the wavelength solution calibrated by ThAr lamp with a 15-GHz astro-comb on the high-resolution spectrograph of the 10-m Southern African Large Telescope. It demonstrates that with the help of the dense and regularly spaced emission lines, the wavelength solution calibrated by astro-comb provides a better characterization of the relation between pixel position and wavelength than that by ThAr lamp.

3.1.2. Asymmetrical Sampling Correction

The non-randomly scattering feature of the blue dots, which looks like splashed waves, can be seen in Figure 2. This feature is the result of asymmetrical sampling of the comb lines. It enlarges the difference between the data and the fitted function, thus it needs to be analyzed.

The nature of asymmetrical sampling can be described briefly as follows. As the adjacent comb lines overlap, a comb line's wings will be non-negligibly raised by its neighboring comb line's wings, making the shape of comb line's wings deviate from the LSF profile (deformation). On the other hand, the comb lines cannot always locate at the center or the edge of a CCD pixel. If the CCD pixels do not sample the comb line symmetrically, the deformation rate included in the CCD sampled data of one wing will be unequal to that of the other wing. It will lead to a systematic bias when the line center is determined by fitting the comb line with our model.

Using the LSF model of HRS to generate a series of comb lines, and setting a particular pixel array to sample them, the asymmetrically sampled overlapping comb lines can be simulated. By fitting one of the simulated comb lines, the systematic bias can be obtained by comparing the fitted line center with the true line center of the LSF profile. Obviously, the spacing between adjacent comb lines in the unit of FWHM plays a key role in asymmetrical sampling, which describes the extent of overlapping. In addition, the extent of asymmetrical sampling also depends on the location of the line center within the pixel, i.e., the pixel phase. Therefore, the systematic bias as a function of the pixel phase has to be examined for different spacing. Here, the pixel phase is expressed by the fraction part of its position: $\phi_x = x - \text{int}(x + 0.5)$ (Anderson & King 2000). Figure 3 shows our analysis result. These four subfigures correspond to the conditions in which the spacing between adjacent comb lines is 3, 2.5, 2 and 1.5 times FWHM of the LSF, respectively. In each subfigure, the relation between the pixel phase and the systematic bias is shown. The locations of the maximum and minimum of the curve are marked with the symbols of "L" and "R". They respectively correspond to left-most and right-most asymmetrical sampling cases, which are illustrated in the two diagrams embedded in the upper part of each subfigure (where the midline of sampling region left-most or right-most deviates from the the true comb-line center). Comparing these four subfigures, it is plain to see that the systematic bias becomes larger as the comb-line spacing decreases. And the amount of bias approaches the level of the absolute calibration rms error, making it necessary to perform the correction.

The process of correcting systematic bias of actual comb lines is almost the same as that described above, but substituting the actual comb-line spacing and pixel phase to simulate the asymmetrically sampled overlapping comb lines rather than surveying the parameter space. The lower panel of each order in Figure 2 shows the residuals of the comb-line centers' wavelength from the new fitted function after correction (shown in green dots). As can be observed, the non-randomly scattering feature is effectively suppressed, and an average 0.00054 Å (27 m s^{-1}) rms error for these five orders is obtained. On the other hand, the residuals of pixel numbers larger than 3500 display an increasing deviation from zero toward the right end in some orders. We find that it is due to the gradual deterioration of the optical aberration

[5] The rms errors in m s^{-1} units in Section 3.1 are all calculated based on 6000 Å, which is the center wavelength of the 470–720 nm wavelength coverage of the astro-comb.

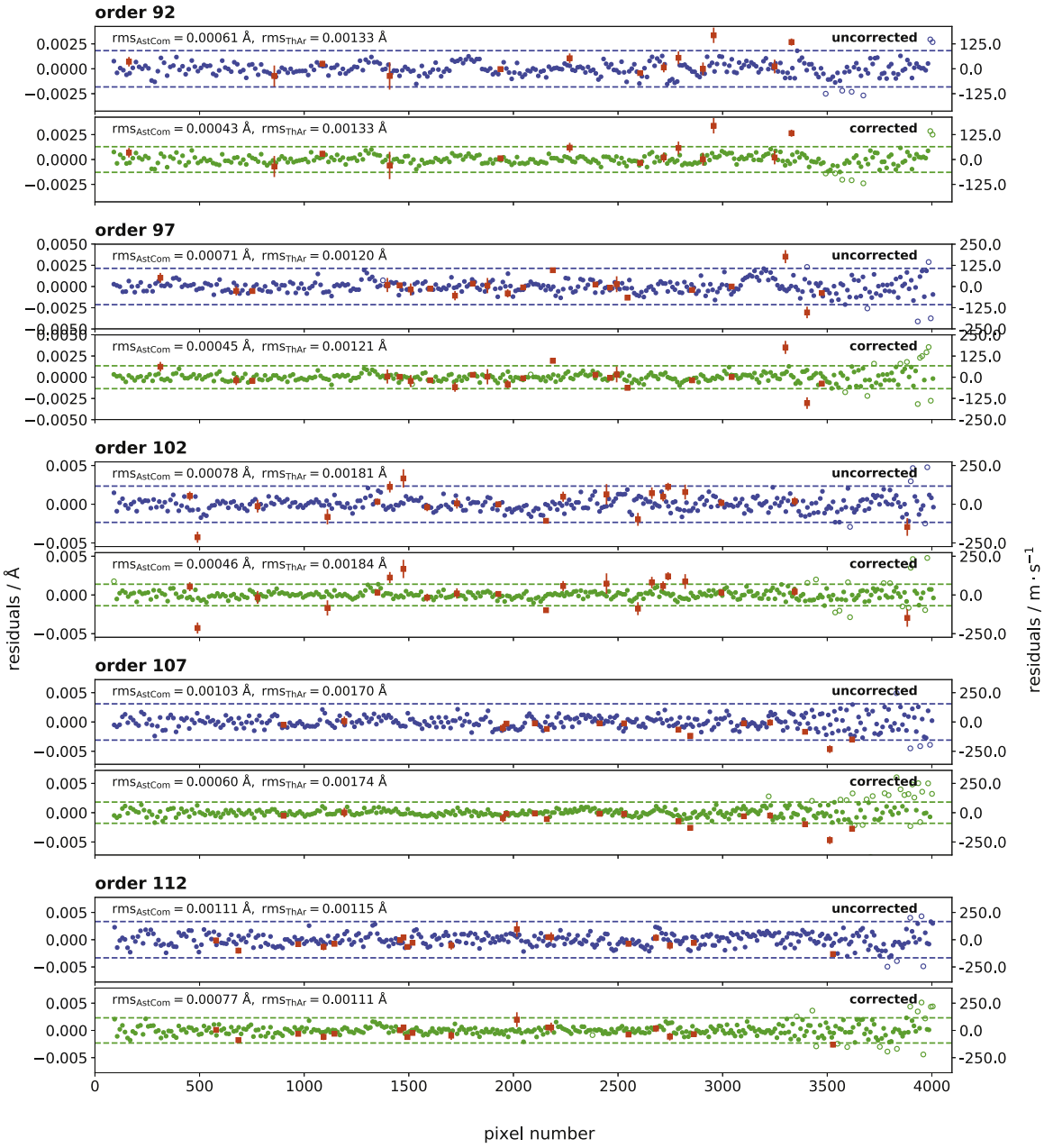

Figure 2. Residuals to the astro-comb's wavelength solution for order 92, 97, 102, 107, 112. For each order, the upper panel shows the result merely after basic absolute calibration process (uncorrected), with the residuals for comb lines shown in blue dots, those for ThAr lamp lines shown in red dots. The lower panel shows the result after asymmetrical sampling correction, with the residuals for comb lines shown in green dots for comparison (those for ThAr lamp lines still shown in red dots). The solid dots indicate the comb lines used to fit, while the hollow dots indicate the discarded comb lines by σ-clipping criterion with $\sigma_{\rm clip} = 3$. The rms error for comb lines ($\rm rms_{AstCom}$) and for ThAr lamp lines ($\rm rms_{ThAr}$) are shown in each panel. The dashed lines indicate $\pm 3\rm rms_{AstCom}$. The error bars for ThAr lamp lines are determined by the propagation of the measured wavenumber uncertainty provided by Table 6 in Redman et al. (2014) and the photon-noise-induced uncertainty in the emission-line fitting.

(A color version of this figure is available in the online journal.)

toward the right end, and this optical aberration is not taken account of in the data reduction process. The find of the negative influence of this optical aberration demonstrates the astro-comb's capability as a diagnostic tool. The residuals for ThAr lamp lines' wavelength from the new fitted function are also plotted (shown also in red dots), showing an average 0.00145 Å (73 m $\rm s^{-1}$) rms error for these five orders, almost with no change. It shows the asymmetrical sampling correction does not introduce systematic global deviation to the wavelength solution.

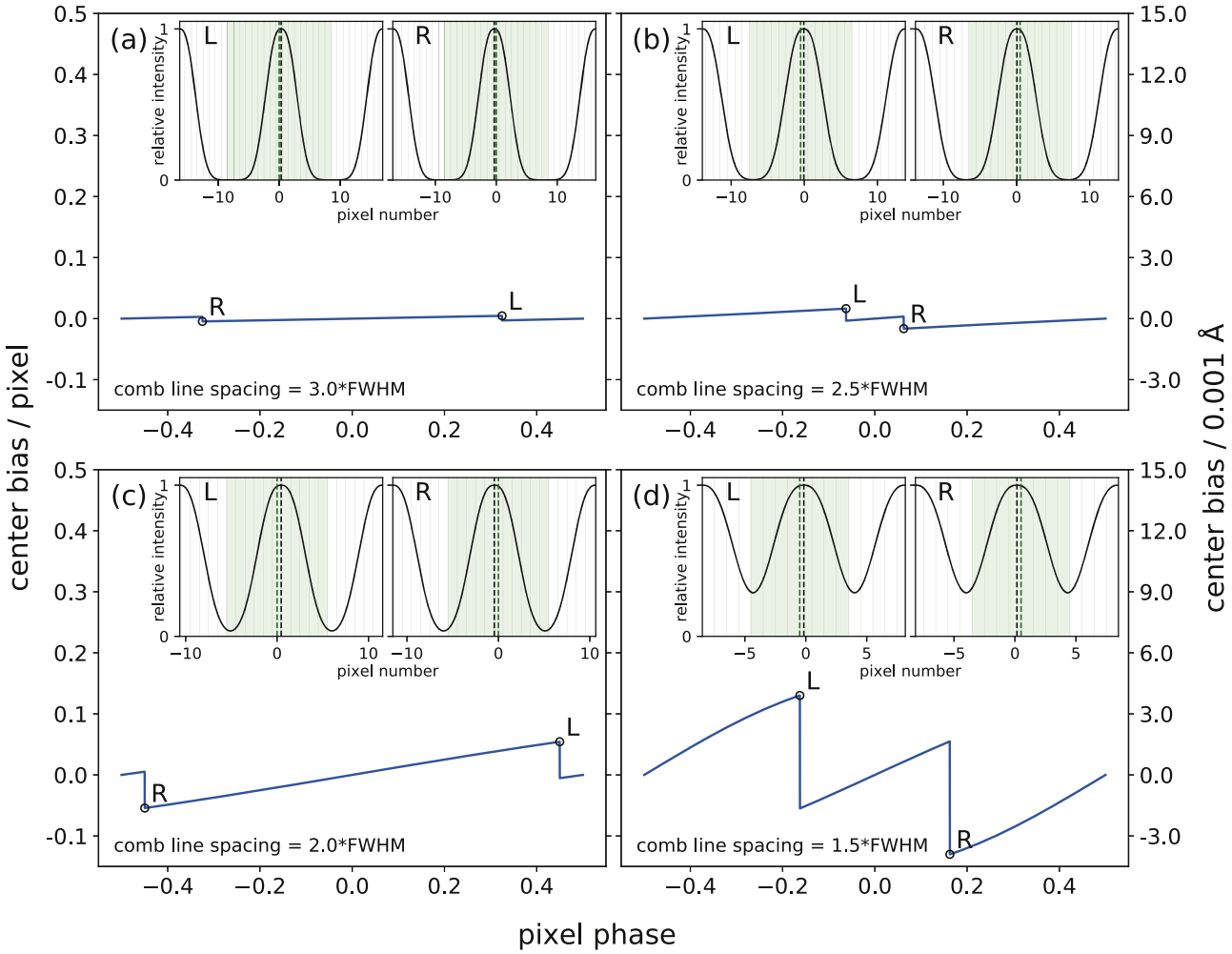

Figure 3. Relation between the pixel phase and the systematic bias caused by asymmetrical sampling. The four subfigures show the comparison of the conditions that the spacing between adjacent comb lines are (a) 3, (b) 2.5, (c) 2 and (d) 1.5 times FWHM of the LSF. The FWHM of the LSF of HRS is 5.5 pixels. The locations of the maximum and minimum of the curve are marked with the symbols of "L" and "R". They respectively correspond to left-most and right-most asymmetrical sampling cases, which are illustrated in the two diagrams embedded in the upper part of each subfigure (where the midline of sampling region left-most or right-most deviates from the the true comb-line center). The edges of each pixel are marked by bars, and the sampling region is filled with light green shadow. The midline of the sampling region is marked by a green dashed line. The true comb-line center is marked by a black dashed line.
(A color version of this figure is available in the online journal.)

An alternative method to mitigate the systematic bias is to fit each comb line by including the two neighboring comb lines in a simultaneous fitting (i.e., three-line simultaneous fitting). However, the effect of implementing this method on our data is not better than one-by-one fitting together with subsequent systematic bias correction. We suspect the imperfect matching between the fitting function and the LSF has influence on the three-line simultaneous fitting. (In this paper, without a set of accurate LSF models accounting for different wavelength, we followed the conventional route to use the Gaussian function to fit the LSF.) The LSF models and their involvement in three-line simultaneous fitting would be investigated in the future.

3.1.3. Photon Noise Limit

The photon noise limit of absolute calibration can be obtained by calculating the standard deviation (SD) of the uncertainties of the line centers for each order under the photon noise assumption. If all the error sources except the photon noise are well suppressed, the absolute calibration precision should be around its photon noise limit. As shown in Figure 4, after asymmetrical sampling correction, the rms error of each order is closer to the photon noise limit. This result shows the excellent effect of the asymmetrical sampling correction. Comparing with ThAr lamp calibration result of 0.003 Å (150 m s^{-1}), a 2–8 times (for different orders) higher

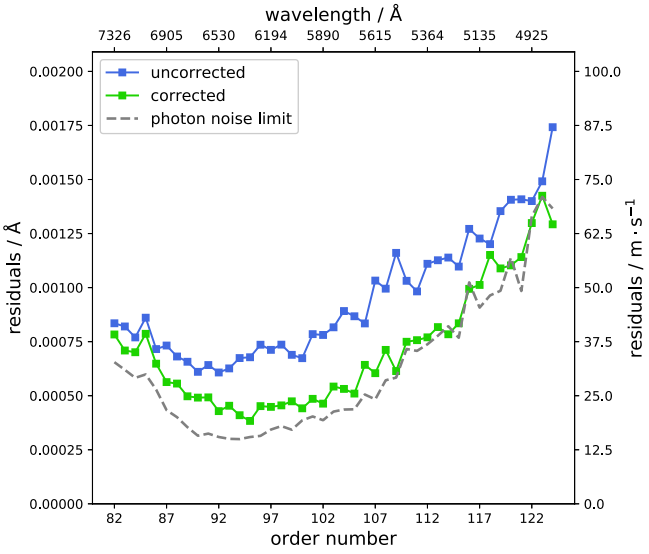

Figure 4. The rms error of the astro-comb's wavelength solution for each order. The result merely after basic absolute calibration process (uncorrected) is shown in blue. The result after additional asymmetrical sampling correction is shown in green. The photon noise limit of the wavelength solution for each order is shown by a dashed line.
(A color version of this figure is available in the online journal.)

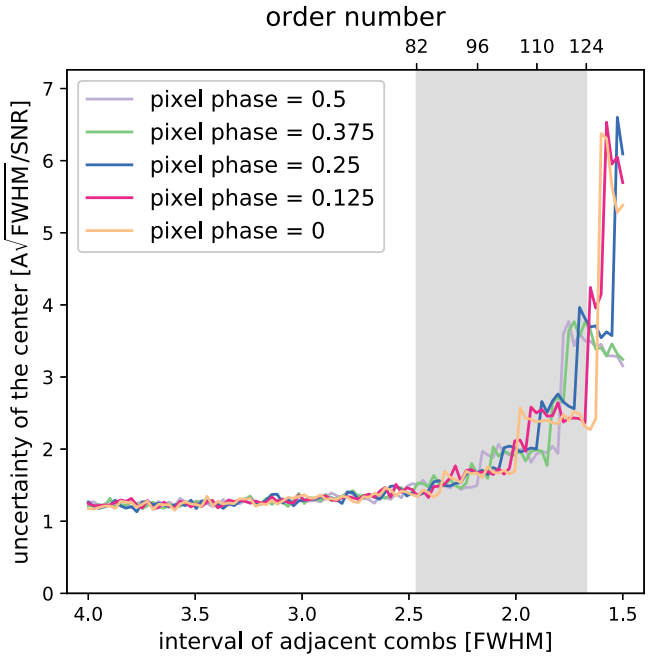

Figure 5. Relation between the comb-line spacing and the uncertainty of the fitted line center for different pixel phases. The uncertainty is in units of $A\sqrt{\mathrm{FWHM}}/\mathrm{S/N}$, where $A = 0.41$ for the Gaussian case (see the text for a detailed description). The FWHM of the LSF of HRS is 5.5 pixels. The result shown in The shadow area marks the range of comb-line spacing for the actual astro-comb on HRS.
(A color version of this figure is available in the online journal.)

wavelength solution accuracy is obtained. The comb lines with higher S/N can provide more precise parameters (comb-line spacing and pixel phase) to the correction process, making the correction process less affected by the noise. Therefore, the correction effect is positively correlated with the S/N of comb lines. Figure 4 shows that better correction effect is obtained in the middle part of the astro-comb's spectral coverage, where the intensity of comb lines is stronger. But for a single exposure, the correction effect is limited by the dynamic range of CCD, which restricts the S/N we can obtained. Figure 4 shows that the discrepancies between the rms error and the photon noise limit still exit.

It should also be noted that the photon noise limit curve is U-shaped in Figure 4. One reason for this curve shape is the envelope shape of the astro-comb's spectrum. Weaker intensity of comb lines toward both ends of the spectrum will lead to larger uncertainties of line centers. Another reason, which mainly influences the right half of the U-shaped curve, is the severer comb-line overlapping in higher orders, where the comb-line wings cannot be well sampled (as shown in the diagrams in the upper parts of Figures 3(c) and (d)). Simulating the overlapping comb lines as in Section 3.1.2, the relation between the spacing of adjacent comb lines and the uncertainty of the fitted line center can be analyzed by Monte Carlo method under the photon noise assumption. The analysis result is plotted in Figure 5. The uncertainty is in units of $A\sqrt{\mathrm{FWHM}}/\mathrm{S/N}$, which is the theoretical prediction of the uncertainty of the fitted line center for fitting a single emission line, where A is set to 0.41 for Gaussian case (Murphy et al. 2007, the form of this formula in our paper is in units of pixels.). Figure 5 shows that the uncertainty increases monotonically with decreasing spacing. Toward the left end, the uncertainty asymptotically converges to a particular value. This value is close to 1, but still a little larger because our line fitting uses five parameters and the LSF is not perfectly Gaussian. Toward the right end, from 2.5 times FWHM to 1.5 times FWHM, the uncertainty drastically increases by several times, though for different pixel phases the curve shapes vary slightly. The range of comb-line spacing for the actual astro-comb is marked by the shadow area in Figure 5. A similar curve shape compared with the right half of the U-shaped photon noise limit curve in Figure 4 can be found. It means that for determination of the line center, the comb line overlapping not only leads to the systematic bias caused by asymmetrical sampling, but also leads to larger uncertainties. Murphy et al. (2007) has demonstrated the fast increase calibration error with decreasing spacing below 3 times FWHM in their analysis of repeatability performance of astro-comb (Figure 4 in Murphy et al. 2007). Our result shows a similar relation from the perspective of absolute calibration. The larger uncertainties mean worse precision. Both the calibration and diagnosis performance of the astro-comb are thus worsened by the more uncertain comb lines. Nevertheless, even for order 124, the average spacing of which is only 1.7 times FWHM,

the accuracy of wavelength solution can still reach 0.0014 Å (70 m s^{-1}). This means an improvement by a factor of two compared with ThAr lamp. The advantage of the astro-comb is still evident.

3.2. Repeatability

The limited stability of spectrograph leads to irregular spectral drift with time. The spectrum of calibration source, which is not exposed simultaneously with the spectrum of the target source, cannot accurately track the spectrograph drift. To avoid temporal separation, the common scheme to carry out the repeatability test is the two-channel simultaneous calibration: the light of calibration source is simultaneously exposed through both the two channels of the spectrograph, forming two separate spectra on the CCD. One spectrum is to trace the spectrograph drift, while the other spectrum is to test the repeatability by comparison with the former. This scheme is not applicable here because the two-channel system of HRS still needs further adjustments. Only the single-channel system is ready for use at the present time. Probst et al. (2015) proposed that in single-channel systems the astro-comb's repeatability can be obtained by dividing the comb lines into groups and measuring the consistency between different groups' RV shifts. The measured repeatability will include all its random components (e.g., photon noise, random spectral instability of comb teeth), which commonly dominates the short-term repeatability, and part of its systematic errors. According to Probst's scheme, odd–even mode calibration and neighboring order calibration are adopted to study the astro-comb's repeatability on HRS. Their methods and results will be presented in the 1st and 2nd parts of this subsection.

In practical observations, in the case of emission-line-type calibration sources (e.g., astro-comb, ThAr lamp) on a single-channel spectrograph, the common scheme to calibrate the RV shift of the scientific target's spectrum is the "time-interlaced calibration" (Probst et al. 2015). Therefore, the repeatability test based on time-interlaced calibration was also carried out. The method and result will be presented in the 3rd part of this subsection.

3.2.1. Odd–even Mode Calibration

Method. To conduct the repeatability test based on odd–even mode calibration, first a series of exposures of the astro-comb are taken. For each exposure, the comb lines are divided into two groups according to their mode numbers: one group constituted of the comb lines with odd mode numbers and the other group of comb lines with even mode numbers. Then, for each exposure, the shifts of both groups from the reference exposure are calculated, respectively, by weighted averaging:

$$\Delta v_{\mathrm{odd},n} = \frac{\sum_i w_{ni}\ (\mu_{ni} - \mu_{1i})\ \frac{c}{\lambda_o(\mu_{ni})}\ \frac{\mathrm{d}\lambda_o(x)}{\mathrm{d}x}|_{x=\mu_{ni}}}{\sum_i w_{ni}} \quad (i = \text{odd mode number}), \tag{2}$$

$$\Delta v_{\mathrm{even},n} = \frac{\sum_j w_{nj}\ (\mu_{nj} - \mu_{1j})\ \frac{c}{\lambda_o(\mu_{nj})}\ \frac{\mathrm{d}\lambda_o(x)}{\mathrm{d}x}|_{x=\mu_{nj}}}{\sum_j w_{nj}} \quad (j = \text{even mode number}), \tag{3}$$

where n denotes the exposure number, thus $\Delta v_{\mathrm{odd},n}$ and $\Delta v_{\mathrm{even},n}$ denote the shifts of the odd-mode and even-mode group for the nth exposure, in the unit of m s^{-1}. μ_{ni}, μ_{nj} are the comb-line centers of mode number i, j for the nth exposure. The first exposure of the series is assigned as the reference exposure. Thus, μ_{1i} and μ_{1j} are subtracted from μ_{ni} and μ_{nj}. $(\mu_{ni} - \mu_{1i})$ and $(\mu_{nj} - \mu_{1j})$ are weighted by their respective inverse variances. According to the theory of the propagation of error, the weights of $(\mu_{ni} - \mu_{1i})$ and $(\mu_{nj} - \mu_{1j})$ can be determined:

$$w_{ni} = \frac{1}{\sigma^2_{\mu,ni} + \sigma^2_{\mu,0i}}, \tag{4}$$

$$w_{nj} = \frac{1}{\sigma^2_{\mu,nj} + \sigma^2_{\mu,0j}}, \tag{5}$$

where $\sigma_{\mu,ni}$, $\sigma_{\mu,0i}$, $\sigma_{\mu,nj}$, $\sigma_{\mu,0j}$ are the uncertainties of μ_{ni}, μ_{0i}, μ_{nj}, μ_{0j} which have been obtained in the comb-line fitting. The agreement between $\Delta v_{\mathrm{odd},n}$ and $\Delta v_{\mathrm{even},n}$ reveals the nature of the repeatability of the astro-comb on HRS. For a series of exposures, the SD of $(\Delta v_{\mathrm{odd},n} - \Delta v_{\mathrm{even},n})$ (denoted by $\sigma_{\mathrm{odd-even}}$) is thus calculated to show the extent of this agreement. Basically, $\sigma_{\mathrm{odd-even}}$ is the integral result of a variety of error sources. If all but the photon noise are well suppressed, $\sigma_{\mathrm{odd-even}}$ should be around the photon noise limit (denoted by $\sigma_{\mathrm{odd-even-pn}}$). $\sigma_{\mathrm{odd-even-pn}}$ can be derived by averaging the photon-noise-assumption-based uncertainty $\sigma_{\mathrm{odd-even-pn},n}$ of each exposure:

$$\sigma^2_{\mathrm{odd-even-pn}} = \mathrm{MEAN}(\sigma^2_{\mathrm{odd-even-pn},n}) \tag{6}$$

and according to the theory of the propagation of error, we obtain

$$\sigma^2_{\mathrm{odd-even-pn},n} = \sigma^2_{\mathrm{odd},n} + \sigma^2_{\mathrm{even},n}, \tag{7}$$

$$\sigma^2_{\mathrm{odd},n} = \frac{\sum_i w_{ni} \left(\frac{c}{\lambda_o(\mu_{ni})}\ \frac{\mathrm{d}\lambda_o(x)}{\mathrm{d}x}|_{x=\mu_{ni}}\right)^2}{\left(\sum_i w_{ni}\right)^2}, \tag{8}$$

$$\sigma^2_{\mathrm{even},n} = \frac{\sum_j w_{nj} \left(\frac{c}{\lambda_o(\mu_{nj})}\ \frac{\mathrm{d}\lambda_o(x)}{\mathrm{d}x}|_{x=\mu_{nj}}\right)^2}{\left(\sum_j w_{nj}\right)^2}, \tag{9}$$

where $\sigma_{\mathrm{odd},n}$ and $\sigma_{\mathrm{even},n}$ are the uncertainties of $\Delta v_{\mathrm{odd},n}$ and $\Delta v_{\mathrm{even},n}$, respectively.

$\sigma_{\mathrm{odd-even}}$ is not the repeatability yet. For both $\Delta v_{\mathrm{odd},n}$ and $\Delta v_{\mathrm{even},n}$, only half of the comb lines are summed, so their real uncertainties should be around $\sqrt{2}\times$ repeatability. According to Equation (7) we finally obtain $\sigma_{\mathrm{odd-even}} \simeq 2\times$ repeatability. The repeatability can be obtained by dividing $\sigma_{\mathrm{odd-even}}$ by two.

Due to the limited stability of spectrograph, some systematic errors included in the extracted spectrum vary by time. For example, the asymmetrically-sampling systematic bias of comb lines will deviate from the original value as the spectrograph drift alters the pixel phase of comb lines; the reciprocal linear dispersion will be changed as the refractive index drifts with the air pressure and temperature. Here, we only focus on the short-term repeatability for exempting from correcting the variation of those systematic errors induced by the spectrograph's instability. The spectrograph drift of HRS is less than 50 m s^{-1} for a 1-hour duration, thus its corresponding change of pixel phase is less than 0.04, by which the induced systematic bias is negligible in comparison with the random uncertainty. Therefore, the duration of each test is decided to be less than one hour. Referring to the CCD readout time of 200 s, each test was finally decided to include 10 exposures.

Results. Six repeatability tests were carried out at different times in 2017. Their results are displayed in Figure 6, arranged in the chronological order. The error bars in the bottom subfigure of each test are equal to $\sigma_{\mathrm{odd-even-pn},n}$, which can be derived from Equation (7)–(9). There is a diminishing tendency of $\sigma_{\mathrm{odd-even-pn}}$ as the tests progressed. This is because better evenness of the comb-line intensity was obtained with the improvement of the performance of the astro-comb, leading to higher S/N for one exposure, while avoiding saturation of any comb line. While both the odd and the even modes' spectral shift amounts to several tens m/s, $\sigma_{\mathrm{odd-even}}$ is only around 0.2 m s^{-1} (the repeatability is only around 0.1 m s^{-1}), and the agreement of $\sigma_{\mathrm{odd-even}}$ and $\sigma_{\mathrm{odd-even-pn}}$ can also be confirmed in Figure 6 (by average of the results of the six tests, $\sigma_{\mathrm{odd-even}}$ is larger than $\sigma_{\mathrm{odd-even-pn}}$ by a factor of 1.06). This result demonstrates that the astro-comb's short-term repeatability on HRS can almost reach the photon noise limit, with other relevant error sources well suppressed.

To quantitatively test the effect of the coupling system, we took two groups of successive exposures. For the first group, the astro-comb was linked to HRS through the coupling system. For the second group, only a simple fiber link was set up: the octagonal-cored MMFs of the coupling system were replaced with ordinary circular-cored MMFs, and the vibrator was shut down. Other conditions were kept unchanged as best as we can. Figure 7 shows the comparison of their results. With similar photon noise limit level and similar amplitude of the spectrograph drift, $\sigma_{\mathrm{odd-even}}$ of the first group is only about one-ninth of that of the second group. It demonstrates the astro-comb's repeatability benefits from the coupling system significantly, improving the repeatability to be close to the photon noise limit.

3.2.2. Neighboring Order Calibration

For neighboring order calibration, the comb lines are grouped according to the diffraction orders and the consistency of neighboring orders' RV shifts is measured. The formulae in Section 3.2.1 to calculate spectral shift can also be employed in this case, with only the need to change the summation range according to the diffraction orders. Using the 10 exposures in the fifth test in Section 3.2.1 to carry out this measurement, we find good consistency of neighboring orders' RV shifts. As shown in Figure 8, for each order, the SD of the difference of neighboring orders' RV shifts is around the photon noise limit. Especially for order 92–102, high proximity can also be confirmed when the photon noise limit is as low as 0.5 m s^{-1}. This result once again demonstrates that the astro-comb's short-term repeatability on HRS can almost reach the photon noise limit. For the photon noise limit curve in Figure 8, the increase toward the right end is less drastic than that in the absolute calibration case (see Figure 4). It is attributed to the use of weighted average in the repeatability test. The photon noise limit curve also shows the repeatability of higher diffraction orders is worsened by the larger uncertainties due to comb-line overlapping.

3.2.3. Time-interlaced Calibration

The method of time-interlaced calibration is to calibrate the target source's spectral shift by interpolating the shifts of the calibration source's spectra, which are exposed before and after through the same channel. Due to the spectrograph's irregular spectral drift, the lag between the target source's spectrum and the calibration source's spectrum will produce interpolation errors, by which the repeatability is worsened. The achievable repeatability is also of concern, because it shows the astro-comb's calibration performance for practical observations by this scheme.

The astro-comb exposures of the six tests in Section 3.2.1 are used to carry out the repeatability test based on time-interlaced calibration. The shift of each exposure from the reference exposure is also calculated by weighted averaging as in Section 3.2.1, with only the need to change the summation range to over all the comb lines. Then the spectral shift of each exposure is compared to the linear interpolation of the spectral shifts of the two exposures before and after. The SD of their differences describes the repeatability. Among them, the exposures at the two ends of each test are disregarded, because either the preceding exposure or the following exposure is absent. The result is shown in Figure 9. It displays a SD of 4.63 m s^{-1}, which is only modestly better than the current 6 m s^{-1} RV measurement precision calibrated by the iodine absorption cell and the ThAr lamp, and several dozens of times larger than the

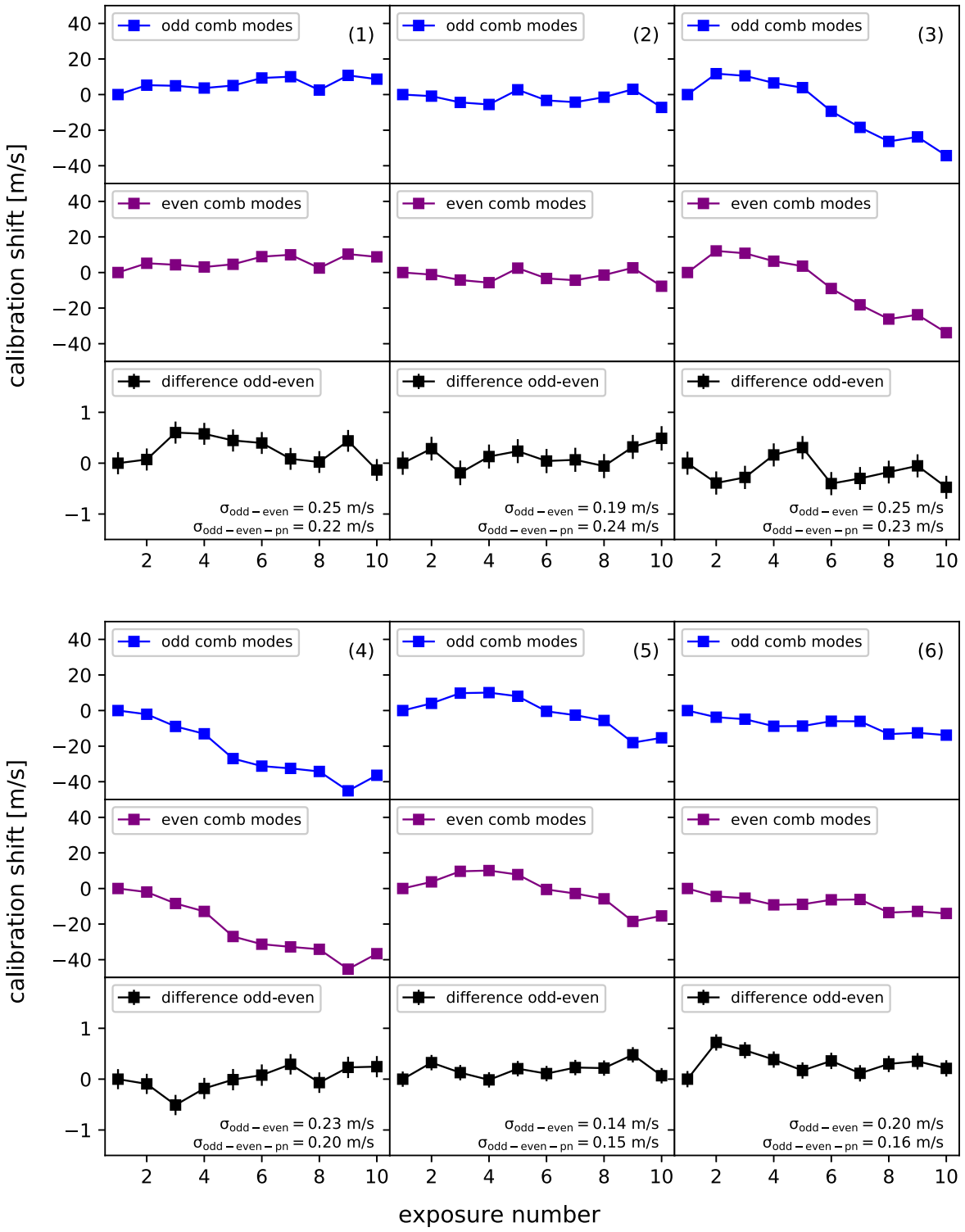

Figure 6. Six repeatability tests of the astro-comb on HRS based on odd–even mode calibration. For each test, the upper panel shows the weighted average shift of the group with odd-mode comb lines ($\Delta v_{\mathrm{odd},n}$), and the central panel shows that of the group with even-mode comb lines ($\Delta v_{\mathrm{even},n}$). The differential shift between the two groups ($\Delta v_{\mathrm{odd},n} - \Delta v_{\mathrm{even},n}$) is shown in the bottom panel. The SD of the differential shift ($\sigma_{\mathrm{odd-even}}$) and the photon noise limit ($\sigma_{\mathrm{odd-even-pn}}$) are calculated and shown. For each exposure, the integration time is 20 s and the readout time is about 200 s.
(A color version of this figure is available in the online journal.)

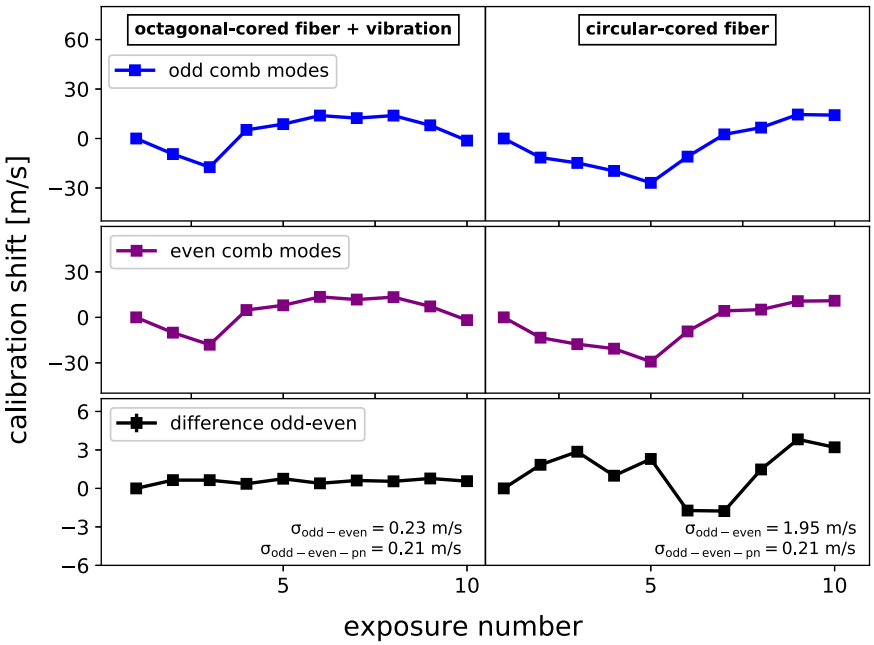

Figure 7. Comparison of the repeatability test results for different fiber link configurations. Left: the astro-comb linked to HRS through the coupling system; right: the octagonal-cored MMFs of the coupling system were replaced with ordinary circular-cored MMFs, and the vibrator was shut down. The implication of each subfigure is explained as in Figure 6. The error bars in the bottom subfigures are still plotted, but they are too short to emerge from behind the square markers.
(A color version of this figure is available in the online journal.)

repeatability performance obtained in Section 3.2.1. This result shows the need of other scheme to better release the potential of the astro-comb for practical observation on HRS.

To improve the precision of practical RV measurements and make better use of the astro-comb, at the current stage, aside from refining the environment control of the spectrograph and the laboratory, a more efficient way is to take advantage of the two-channel system of HRS to simultaneously calibrate the RV shift of the scientific spectrum. Simultaneous calibration can effectively suppress the errors induced by the irregular spectrograph drift. How to maximally reduce the negative influence of the channel crosstalk on the calibration precision is what we need to mainly focus on.

4. Summary

We have successfully installed a 25-GHz mode-spacing broadband visible-wavelength astro-comb as the calibration source on the fiber-fed High Resolution Spectrograph (HRS) of the Chinese 2.16-m telescope at Xinglong Observatory. A coupling system linking the astro-comb with HRS was set up to implement fiber scrambling. The absolute calibration tests and repeatability tests were carried out based on the single-channel system of HRS. The results of those tests have demonstrated the benefit of HRS from the astro-comb: a 2–8 times (for different orders) higher wavelength solution accuracy than the

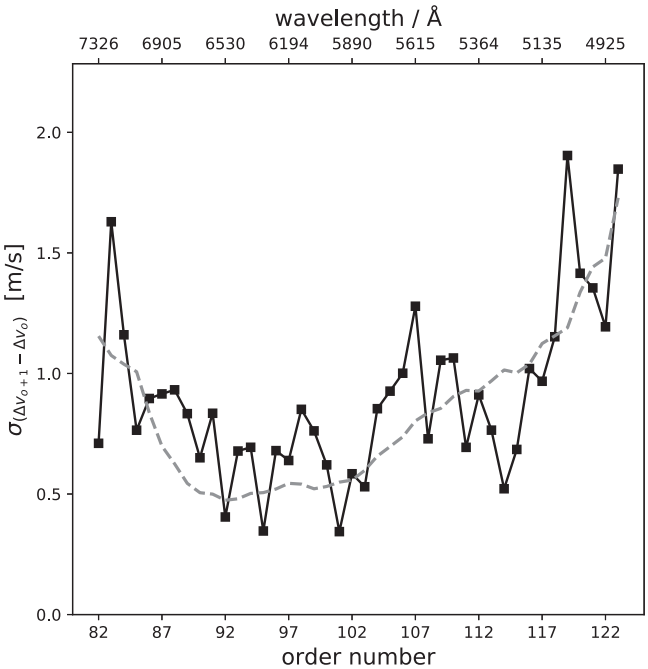

Figure 8. Repeatability tests of the astro-comb on HRS based on neighboring order calibration. Δv_o denotes the spectral shift of order o. $\sigma_{(\Delta v_{o+1}-\Delta v_o)}$ is the SD of the difference between the spectral shift of order $o+1$ and the spectral shift of order o for a series of exposures. Using the ten exposures of the fifth test in Figure 6, each order's $\sigma_{(\Delta v_{o+1}-\Delta v_o)}$ is calculated and shown in solid line. The corresponding photon noise limit is shown in dashed line.

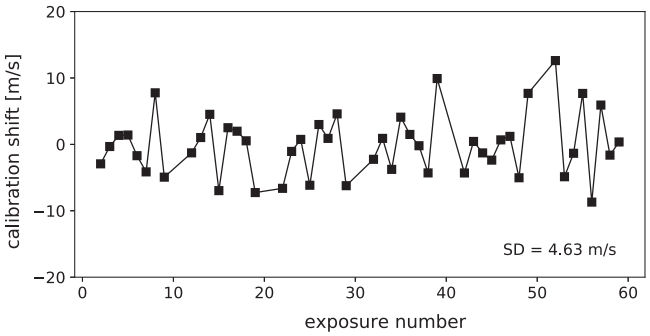

Figure 9. Repeatability tests of the astro-comb on HRS based on time-interlaced calibration. The spectral shift of each exposure is compared to the linear interpolation of the spectral shifts of the two exposures before and after. The difference of them is plotted in solid line, having an SD of 4.63 m s^{-1}.

ThAr lamp and a short-term repeatability of 0.1 m s^{-1}. The short-term repeatability was in good agreement with the photon noise limit. It means except the photon noise all random components of repeatability and relevant systematic errors have been well corrected. It confirms the entire system including HRS and the astro-comb was well-established. The coupling system successfully suppressed the negative effects of laser speckles.

Additionally, the influence of the comb-line overlapping was investigated. We found that when determining the comb-line center, the comb-line overlapping leads to a systematic bias, which is caused by asymmetrical sampling, and meanwhile a larger uncertainty. The correction for the systematic bias is feasible by simulating the overlapping comb lines according to actual comb-line spacing and pixel phase, then calculating the difference of the fitted line center with the true line center. We demonstrated that the accuracy of wavelength solution was improved after correction, and the rms errors of some orders have almost been as low as the photon noise limit.

The repeatability test based on time-interlaced calibration has shown a limited improvement comparing with the traditional calibration sources. To release the potential of the astro-comb for practical RV measurements, taking advantage of the two-channel system of HRS to simultaneously calibrate the RV shift of the scientific spectrum is our future plan.

We gratefully acknowledge the help of Wang Liang from the Max Planck Institute for Extraterrestrial Physics; Wang Huijuan and Zhao Fei from National Astronomical Observatories, Chinese Academy of Sciences; and Rafael Andreas Probst from Max Planck Institute for Quantum Optics. They gave us many useful suggestions about the data analysis and the programming. We acknowledge the help of Li Hongbin from National Astronomical Observatories, Chinese Academy of Sciences, who helped us finish the system installation on site. We acknowledge the support of the National Natural Science Foundation of China (NSFC) (grant Nos. 11373051, 11503058, 11673046, 11773044, 11803060, and 11873071). Hao Zhibo acknowledges the support of the Opening Project of CAS Key Laboratory of Astronomical Optics & Technology (grant No. CAS-KLAOT-KF201701).

References

Anderson, J., & King, I. R. 2000, PASP, 112, 1360
Brucalassi, A., Grupp, F., Kellermann, H., et al. 2016, Proc. SPIE, 9908, 99085W
Charsley, J. M., McCracken, R. A., Reid, D. T., et al. 2017, Proc. SPIE, 10329, 103290Y
Doerr, H.-P., Kentischer, T. J., Steinmetz, T., et al. 2012, Proc. SPIE, 8450, 84501G
Fan, Z., Wang, H.-J., Jiang, X.-J., et al. 2016, PASP, 128, 115005
Liu, Y.-J., Sato, B., Zhao, G., et al. 2008, ApJ, 672, 553
Liu, Y.-J., Sato, B., Zhao, G., & Ando, H. 2009, RAA, 9, 1
McCracken, R. A., Charsley, J. M., & Reid, D. T. 2017a, OExpr, 25, 15058
McCracken, R. A., Depagne, E., Kuhn, R. B., et al. 2017b, OExpr, 25, 6450
Molaro, P., Esposito, M., Monai, S., et al. 2013, A&A, 560, 61
Murphy, M. T., Udem, Th., Holzwarth, R., et al. 2007, MNRAS, 380, 839
Phillips, D. F., Glenday, A. G., Li, C.-H., et al. 2012, OExpr, 20, 13711
Probst, R. A., Wang, L., Doerr, H.-P., et al. 2015, NJPh, 17, 023048
Probst, R. A. 2015, PhD thesis, Ludwig Maximilian Univ. of Munich
Probst, R. A., Lo Curto, G., Avila, G., et al. 2016, Proc. SPIE, 9908, 990864
Redman, S. L., Nave, G., & Sansonetti, C. J. 2014, ApJS, 211, 4
Sato, B., Wang, L., Liu, Y.-J., et al. 2016, ApJ, 819, 59S
Skidmore, W. & TMT International Science Development Teams, & TMT Science Advisory Committee. 2015, RAA, 15, 1945
Steinmetz, T., Wilken, T., Araujo-Hauck, C., et al. 2008, Sci, 321, 1335
Tody, D. 1993, ASPC, 52, 173
Wang, L., Sato, B., Zhao, G., et al. 2012, RAA, 12, 84
Wang, L., Sato, B., Omiya, M., et al. 2014, PASJ, 66, 118
Wang, L., Grupp, F., Kellermann, H., et al. 2016, Proc. SPIE, 9913, 99133O
Wilken, T., Lovis, C., Manescau, A., et al. 2010, Proc. SPIE, 7735, 77350T
Wilken, T., Lo Curto, G., Probst, R. A., et al. 2012, Natur, 485, 611
Wu, Y.-J., Ye, H.-Q., Han, J., et al. 2016, Acta Optica Sinica, 36, 0614001
Ycas, G. G., Quinlan, F., Diddams, S. A., et al. 2012, OExpr, 20, 6631
Ye, H.-Q., Han, J., Wu, Y.-J., & Xiao, D. 2016, Proc. SPIE, 9908, 99087E
Zhao, F., Zhao, G., Lo Curto, G., et al. 2014, RAA, 14, 1037